RESEARCH ARTICLE

Particle velocimetry inside Newtonian and non-Newtonian droplets impacting a hydrophobic surface

M. I. Smith · V. Bertola

Abstract A particle velocimetry technique is described which enables the measurement of the fluid velocity inside impacting drops. Using high speed photography of 2 μm fluorescent tracer particles suspended in the fluid, the velocity field was measured as a function of time and radial position. The potential of the technique is illustrated using velocimetry measurements of drops of pure water and aqueous solutions of 200 ppm poly-(ethylene oxide) (PEO). Dilute solutions of PEO have been known for some time to suppress the rebound of water from hydrophobic surfaces. The dissipation has traditionally been attributed to an increased extensional viscosity as the polymers stretch in the extensional flow of the droplet. Our results enable us to infer that the extensional viscosity of PEO drops, during both the spreading and retraction phase, is similar to that of pure water. The data suggest that the true source of dissipation lies at the droplet edge. We also show, by analysing the spreading of water drops, that the Roisman-Yarin theory for a droplet spreading on a surface is valid in the bulk of the droplet prior to the final stages of spreading.

M. I. Smith · V. Bertola (✉)
SMART Laboratory, University of Edinburgh, King's Buildings,
Mayfield Rd, Edinburgh, UK
e-mail: v.bertola@ed.ac.uk

Present Address:
M. I. Smith
Department of Physics and Astronomy, University
of Nottingham, University Park, Nottingham, UK
e-mail: mike.i.smith@nottingham.ac.uk

1 Introduction

Particle Image Velocimetry (PIV) has been a recognised technique for 25 years (Westerweel 1997; Tropea et al. 2007; Adrian 2005) and in that time has become an indispensable tool for visualising and quantifying fluid flows. Initial research in the field used laser speckle patterns, generated by particles suspended in the fluid. The phase difference between randomly distributed particles creates an interference or speckle pattern. As the position of particles move with the fluid, the speckle pattern shifts with them allowing the fluid motion to be measured. This technique has been developed and applied to a large variety of laminar and turbulent flows including multiphase flows (e.g., Bertola 2003 and references therein).[1]

An alternative method of measuring fluid velocity, and the one which is followed here, is to resolve and track the positions of individual particles, which is known as Particle Tracking Velocimetry (PTV). Provided the particles faithfully follow the flow, the velocity of the particles can be understood to be the same as that of the suspending fluid, a condition that is satisfied for small particles of similar density to the fluid at relatively low fluid velocities (Adrian 1991). The particles therefore move along the fluid pathlines enabling the motion to be observed and quantified. In comparison with PIV, PTV allows one to achieve much higher spatial resolution without increasing significantly the particle concentration, which would be necessary to obtain PIV speckle patterns.

Droplet impact on a solid substrate represents an intriguing class of fluid flows. Commercial and academic interest in the field has driven a sizeable research effort,

---

[1] For a detailed description of this and other methods of particle image velocimetry see the excellent review by Adrian (1991).

focussed on understanding and controlling droplet deposition (Yarin 2006; Rein 1993). Applications are as diverse as inkjet printing, spray cooling, soldering of microelectronics, forensic science and the agrochemical industry (Yarin 2006; Berberovic et al. 2009; Williams et al. 2008). Despite the apparent importance of understanding drop impact, measurement techniques have to date been largely focussed on macroscopic observables such as the velocity of the contact line or the drop shape (e.g., Bergeron et al. 2000; Crooks et al. 2001). Drop impact has therefore been unable to benefit from the same insights provided by particle imaging in other areas of fluid dynamics. Whilst the literature reports various theoretical models (Roisman 2009; Yarin and Weiss 1995; Roisman et al. 2001) and the relative numerical solutions (Eggers et al. 2010; Sikalo et al. 2005; Fukai et al. 1993), there is little experimental data to enable these models to be adequately validated in the drop interior.

Drop impact presents certain specific difficulties that make measurement of the fluid flow inside the droplet a challenging problem. Firstly, since a droplet is a few millimetres in diameter, the tracer particles used to track fluid flow must be small ($\sim\mu m$). This requires observations to be made at high magnification. The shape of a small droplet with surfaces of changing curvature adds to the difficulty of making accurate measurements due to refraction and reflection (Bertola 2003). Ray tracing methods have been developed and used to some success to overcome these limitations for sessile droplets (Kang et al. 2004) and an early attempt at PIV measurements was carried out in acoustically levitated droplets (Yarin et al. 1999). Yet such methods would be extremely difficult to implement during the significant deformations associated with drop impact. Secondly, there is the issue of time scale: droplet impact is a fast process with complete spreading of the droplet occurring in just a few milliseconds. With a fluid velocity of 1,000 mm/s followed at a magnification of 40x with a typical field of view of ~ 0.5 mm, a 2-micron particle crosses the entire field of view in just 0.5 ms. However, to record the discrete position of a particle using a megapixel camera, one needs exposure times of order one thousand times shorter than this. At such short exposure times, achieving sufficient illumination is also an important consideration.

During drop impact onto smooth and chemically homogeneous surfaces, and for low or moderate impact kinetic energy, the dynamics are controlled by three key factors: inertia, viscous dissipation and interfacial energy (Rein 1993; Yarin 2006). During the initial stages of impact with the surface, the vertical inertia of the falling drop is converted into the horizontal motion of the fluid. Surface tension can also be important depending on the relative magnitude of both terms. This balance is characterised by the dimensionless Weber number ($\rho V_i^2 D_0/\sigma$). As the fluid spreads across the surface, the kinetic energy of the fluid is partly dissipated by viscous forces in the fluid. The extent to which viscous dissipation is important in governing drop dynamics is described using the Reynolds number ($\rho V_i D_0/\eta$) which is sometimes used in combination with the Weber number to yield the Ohnesorge number ($\mathrm{We}^{0.5}/\mathrm{Re}$). Finally, as the drop reaches maximum spreading, surface tension slows expansion storing the remaining kinetic energy of the fluid in the interfacial energy generated through drop deformation. At this point, a drop will have the shape of a disc (eventually surrounded by a circular rim), commonly known as a "lamella". Provided the splashing threshold is not exceeded, which is true in the case of our experiments, the disc then begins to retract as the stored interfacial energy is released. If the effects of surface roughness can be neglected, this retraction is governed by a balance between interfacial energy and the viscous dissipation, Capillarity ($V_{\mathrm{retraction}}\eta/\sigma$) (Rein 1993; Yarin 2006). Importantly, in the context of the present study, this means that if two drops with similar size, density, velocity and surface tension impact a surface, one expects the difference in fluid velocity during spreading is related to the kinematic viscosity. Similarly if two drops with the same interfacial energy spread to form discs of the same diameter on identical surfaces (ie with the same chemical structure and the same surface roughness), differences in the initial retraction velocity, all other factors being equal, are determined by the fluid viscosity.

If the fluid retracts with sufficient velocity, it rises in the middle forming a Worthington jet which may subsequently result in the complete rebound of the drop from the surface. It has been known for many years that the addition of a small quantity of a flexible polymer to the fluid completely suppresses rebound (Bergeron et al. 2000). This is due to the reduction in retraction velocity of the lamella by one order of magnitude compared to the drop of pure water. However, a dilute polymer solution has a shear viscosity and surface tension similar to that of pure solvent (Crooks et al. 2001; Bertola 2004; Bertola 2009), making such a dramatic difference in behaviour surprising.

Under a strong elongational velocity gradient, polymers in a random coil experience a differential drag, resulting in a transition to a stretched out state (coil-stretch transition) (de Gennes 1974; Keller and Odell 1985). From a macroscopic point of view, the ensemble of molecules undergoing a coil-stretch transition causes an increase in the so-called extensional (or elongational) viscosity, the ratio of the normal stress difference to the extension rate. A droplet spreading on a surface results in an elongational flow, and hence, it was proposed that this temporary change in the extensional viscosity dissipated sufficient energy to prevent droplet rebound.

Several problems have however been identified with this interpretation. Firstly, the velocity of the contact line during spreading is found to be the same for both the water and PEO drop. Secondly, when interfacial effects are removed by impact on small targets or heated surfaces the retraction velocity of water and PEO drops are similar (Bertola 2004, 2009; Rozhkov et al. 2003). However, these measurements are indirect, measuring purely the drop diameter and not the bulk of the drop.

Here, we describe a novel experimental technique which enables measurements of the fluid velocity as a function of time and radial position to be performed on an impacting droplet. We subsequently apply this technique, comparing the fluid velocity inside water and viscoelastic drops (200 ppm PEO water solution), allowing a better understanding of the anti-rebound effect mechanism (Smith and Bertola 2010).

2 Experimental set-up and technique description

Our experimental set-up is shown schematically in Fig. 1. The system is constructed around an inverted microscope (Axiovert 200, Zeiss) containing a $40\times$ microscope objective (NA 0.75, Plan-NeoFluar, Zeiss) which was chosen for its low autofluorescence. Illumination is provided by a pulsed UV laser (365 nm, mean power ~ 5 mw , Photonics Solutions) which produces ~ 1 ns pulses at a frequency of ~ 8 kHz. The laser is mounted on a fully adjustable translation mount. The beam was then collimated and expanded (Thorlabs) and focussed into the rear focal plane of the objective. The light entering the rear of the objective is reflected from a dichroic mirror (FT 510). This resulted in an approximately uniform illumination of the entire visible focal plane. Fluorescence from the focal plane is collected by the same objective before being filtered with a low pass spectral filter (LP 515). The field of view was recorded using a high speed CMOS camera (Phantom V9.1) equipped with a monochrome image intensifier (IL90, Lambert Instruments).

In order to visualise the flow, a small quantity (~ 0.001 wt%) of 2 μm fluorescent tracer particles (Brookhaven) was then added to the fluid. At such low concentrations, the particles have no discernible effect on the droplet impact dynamics but fluoresce brightly when excited by the laser light. Since the diameter of the particles is small, their motion can be understood to faithfully reflect the underlying motion of the fluid (Adrian 2005). Drops were formed using a syringe gauge at the end of a blunted hypodermic needle and detached under their own weight. The properties of the two types of drop are summarised in Table 1. The hypodermic needle was carefully positioned above the objective using a micrometre adjusted mount. The mount enabled the needle
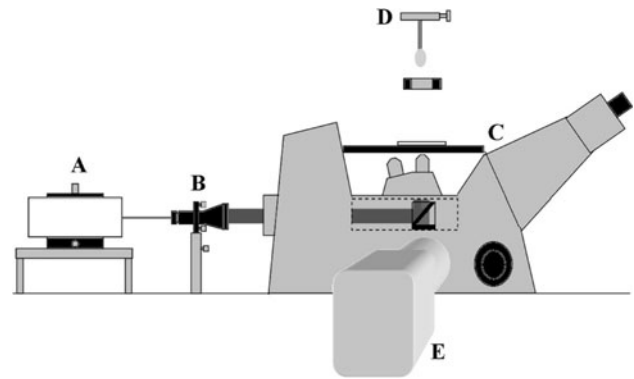

Fig. 1 Schematic of the experimental set-up. *A* A pulsed UV laser is used to excite 2 μm fluorescent colloids inside an impacting water droplet. *B* The beam is collimated and expanded by an adjustable beam expander. *C* The beam is reflected from a dichroic mirror and focussed through a $40\times$ microscope objective. The collected image is filtered using a low pass filter. *D* The drop is created at the end of a blunt needle. As it falls, the drop passes through a light gate which *E* triggers a high speed camera, fitted with image intensifier, to record a movie at 2,000 fps

Table 1 Water and PEO drop properties

Fluid	Water	200 ppm PEO
Drop diameter (mm)	2.76 ± 0.14	2.66 ± 0.1
Density at 20°C (kg/m^3)	1,000	1,000
Viscosity at 20°C (mPa·s)	1	1.23
Surface energy at 20°C (mJ/m^2)	72	70

to be moved radially relative to the objective, allowing the observation of different radial positions within the impacting drop. Above the objective on the microscope stage, a thin glass coverslip (AGAR scientific, #0) coated with a thin film of Fluropel® PFC1302A (Cytonix Corp.) was used as our hydrophobic test substrate (contact angle $\sim 106°$). The plane of focus was set to a height of 10 μm $\pm$ 2 above the glass substrate. The falling drops passed through an optical gate which triggered the high speed camera to collect a series of images at 2,000 fps.

Figure 2 (bottom) shows part of a typical image collected during the spreading of a droplet. Since the laser produces 8,000 pulses per second and the camera records at 2,000 fps, it follows that the single particle shown moving through the field of view was exposed 4 times. Hence, the central diagram in Fig. 2 shows 3 particles each exposed 4 times. Knowing the time between laser pulses, these particle streaks enable us to measure the velocity of the fluid by measuring the distance travelled by each particle ($V_{fluid} = \Delta x_{colloid}/\Delta t_{laser}$). Since the measurements depend quite critically upon the frequency of the laser, the time between pulses was verified in the following way. A small puddle of concentrated fluorescent colloidal solution was
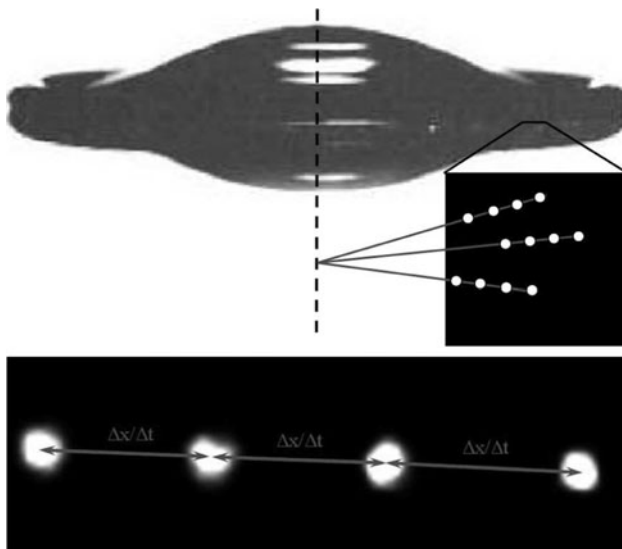
Fig. 2 PIV analysis: *Top* Sideview of a spreading water drop on a hydrophobic surface. *Middle* Diagram showing collection of images at a particular radial position. Colloids appear as bright fluorescent spots each exposed four times by the laser. Hence, the diagram illustrates only 3 colloids. Extrapolation of the radial paths of multiple colloids can be used to find the central point of the drop, and hence, the radial coordinate of each measurement. *Bottom* Part of a typical image of a single fluorescent colloid inside a spreading drop of water. The fluid velocity can be measured since $V_{fluid} = \Delta x_{colloid} / \Delta t_{laser}$

placed on a clean coverslip. The high speed camera was then set to record at a frame rate of 100,000 fps. The number of pulses of light captured in 1,500 frames was then used to determine the laser frequency. The spatial resolution of the microscope was also measured using a calibration standard. The precise impact position of each droplet was found to vary between drops, due to the inherent instability of detachment. However, it was noted that with the exception of the very edge of the spreading droplet, particles followed radial paths during spreading. By calculating the intersection of linear fits to the particle streaks, it was possible to determine the centre of the drop impact, and hence, the radial coordinate for particles within each frame (Fig. 2). Time coordinates were measured relative to the triggering of the camera by the falling drop. By collecting series of images at different radial positions, it was possible to map out the fluid velocity as a function of both time and radius (Figs. 3, 4, 6, 7).

3 A comparison of water and 200 ppm PEO solution

Using this technique, we compared the fluid velocities inside impacting drops of water and dilute solutions of poly-(ethylene oxide) (PEO). PEO, at a concentration of 200 ppm, was slowly dissolved in deionised water which
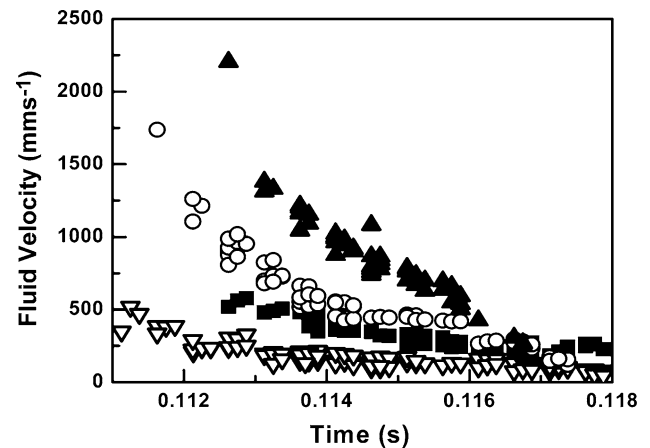

Fig. 3 Particle image velocimetry of water drops impacting a hydrophobic substrate (radii *open inverted triangle* 0.7, *filled square* 1.3, *open circle* 1.6, *filled triangle* 2.8 mm). As time increases, the fluid slows before retracting
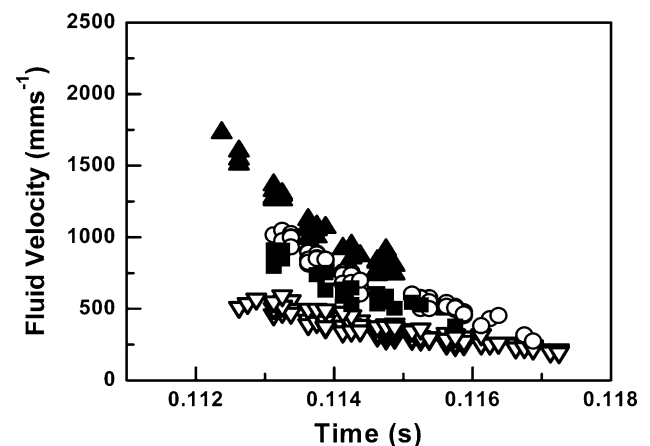

Fig. 4 Particle image velocimetry of 200 ppm PEO drops impacting a hydrophobic substrate (*bottom*, radii *open inverted triangle* 1.2, *filled square* 2.0, *open circle* 2.1, *filled triangle* 2.7 mm). As time increases the fluid slows before retracting

was stirred continuously with a magnetic stirrer. Table 1 summarises the properties of the two fluids used.

Drops were released from a height of 100 mm resulting in an impact speed of $\sim 1,400$ mms^{-1} (We$_{water} \sim 75.1$, We$_{PEO} \sim 74.5$). As the spreading drop passes over the objective, a small increase in the background intensity is observed followed by a series of particles carried along by the fluid. For drops of pure water and those with PEO additives, particles are observed to follow radial paths during spreading. As the fluid slows, a sudden reversal in the direction of the flow is observed as the drop begins to retract. Movies were collected at different radial positions up to about 80% of the maximum spreading radius. Beyond this position, instabilities in the fluid cause particles to

deviate a significant amount from the usual radial paths, making location of the centre of drop impact impossible.

3.1 The spreading stage

Figures 3 and 4 show some example plots of the velocity as a function of time at different radial positions for both water and PEO drops. Upon impact the drop spreads rapidly with the velocity increasing as a function of radius and decreasing as a function of time as is expected. After approximately 0.118 s, the fluid velocity is observed to drop almost to zero.

Considering a momentum balance in the radial direction of the spreading droplet, theory predicts the velocity field inside the lamella should obey $V = r/(t + \tau)$ (Yarin and Weiss 1995; Roisman et al. 2001), for $t \gg D_0/U_0$ (where D_0 is the initial drop diameter and U_0 is the impact velocity). Figure 5 shows the spreading of the water droplet with the radial coordinate divided by the velocity plotted against time. A linear fit to all the data before $t = 0.116$ s is also shown. This clearly indicates the validity of the proposed model not only for the lamella thickness as previously demonstrated (Bakshi et al. 2007) but also in the bulk fluid of the drop. All measurements of time were taken relative to the triggering of a light gate by the falling drop, but a good estimate of the time of impact can be made by observing the movies collected near the centre of the drop. All movies which show the centre of the drop impact indicate drop impact occurs at $t = 0.110 \pm 0.0005$ s. Calculation of the intersection of the line of best fit with $t = 0.110$ s suggests a value of $\tau \sim 0$ within the experimental error. For our system $D_0/U_0 \sim 0.002$ s therefore, we expect to see little departure from a linear fit at small times. As the droplet approaches
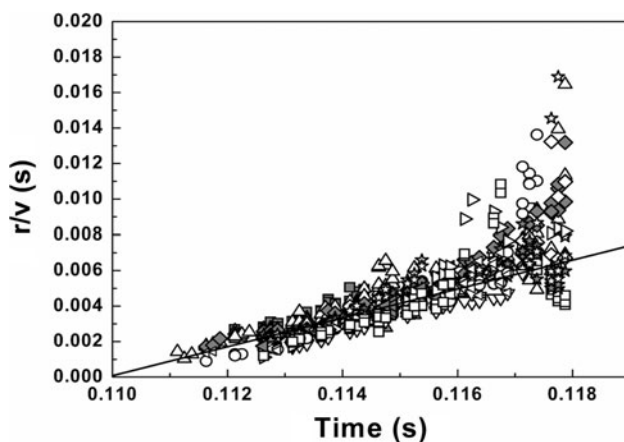
maximum spreading, the velocity approaches its minimum value leading to a deviation from the linear trend.

Comparison of the fluid velocities presented in Figs. 3 and 4 is easier when they are plotted as a function of the radial position for both PEO and water (see Figs. 6, 7). Little difference between the two fluids is apparent. This conclusion is further strengthened by comparing the velocity gradients in the fluid as a function of time (a parameter which determines whether a polymer undergoes a coil-stretch transition) which is shown in Fig. 8. The values observed for the dilute PEO solutions are almost identical to those of water, suggesting similar amounts of dissipation throughout the spreading of the droplet. Since
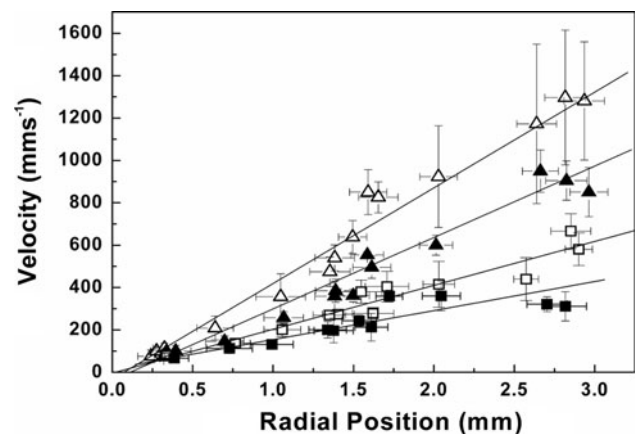
Fig. 6 Velocity profile in the spreading water drop. The measured velocities from each data set are averaged over certain time windows (*open triangle* 0.1125–0.11375, *filled triangle* 0.11375–0.115, *open square* 0.115–0.11625, *filled square* 0.11625–0.1175). The vertical error bars reflect the standard deviations in the measured velocities. The velocity gradient inside the drop is linear at all measured times
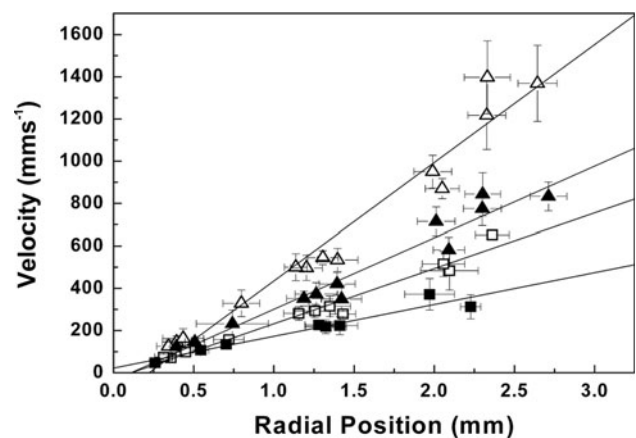
Fig. 5 Validation of the Roisman-Yarin theoretical prediction of the fluid velocity inside the spreading drops (see main text for details). The linear best fit yields $r/v = 0.81t - 0.09$. Drop impact occurs at $t = 0.110$ s

Fig. 7 Velocity profile in the spreading 200 ppm PEO drop. The measured velocities from each data set are averaged over certain time windows (*open triangle* 0.1125–0.11375, *filled triangle* 0.11375–0.115, *open square* 0.115–0.11625, *filled square* 0.11625–0.1175)
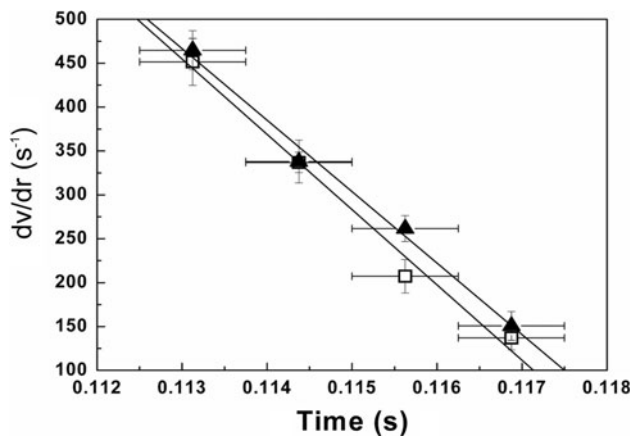
Fig. 8 A comparison of spreading in a water (*open square*) and 200 ppm PEO (*filled triangle*) drop. Both drops exhibit similar velocity gradients with respect to time. Changes in extensional viscosity should be observed through changes in the velocity profile yet both fluids are clearly similar

the two drops have the same impact velocity, surface tension, shear viscosity and density, the only parameter that could cause differences in spreading behaviour is the extensional viscosity caused by polymers stretching in the flow. However, our measurements show that at least in the bulk fluid no such differences are observed. This raises serious doubts about any significant role for extensional viscosity in suppressing droplet rebound. The magnitude of the velocity gradients measured in the fluid appears totally consistent with such an interpretation. Measurements by Crooks et al. (2001) of the Trouton ratio (extensional viscosity/shear viscosity) suggest that no significant increases are observed below extension rates $\sim 1,000$ s^{-1}. It therefore appears that during spreading, at the impact velocities considered, extensional viscosity is not an important parameter.

3.2 The retracting stage

The fluid gains its maximum retraction velocity on a timescale that is comparable with 1 or 2 frames of the captured sequences of images. Observation of the recorded movies appears to show that as the spreading fluid slows almost to zero, a wave of fluid from the edge of the retracting drop sweeps across the field of view leading to a jump in fluid velocity.

Velocity profiles for the retracting PEO drop show significantly smaller fluctuations in the velocity as a function of time. This is consistent with recent direct numerical simulations showing a reduction in small-scale convective motions in dilute polymer solutions (Boffetta et al. 2010). Figures 9 and 10 show the retraction velocity of water and PEO drops. Despite significant scatter in the data, it is clear that radial velocity gradients in both cases are small (ie
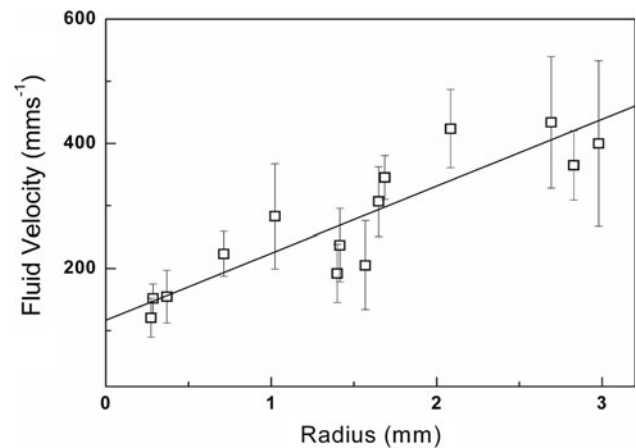

Fig. 9 Retraction velocities inside retracting drops of water. The vertical error bars represent the standard deviation of velocities observed during the initial retraction of the drop for each experiment
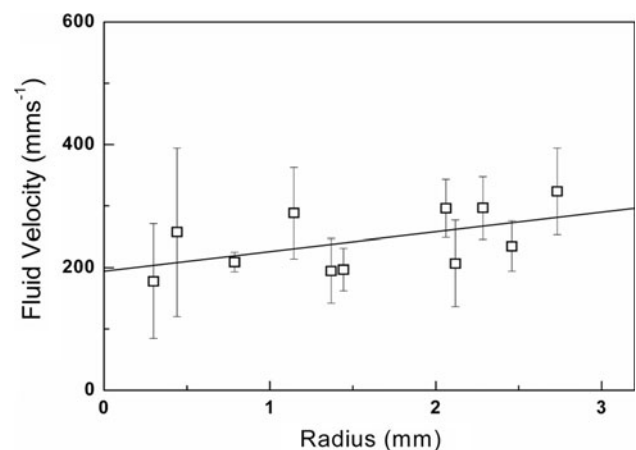

Fig. 10 Retraction velocities inside retracting drops 200 ppm PEO solution. The fluid velocity inside PEO drops is similar to that of water drops, providing direct evidence that the elongational viscosity of both drops is not responsible for the anti-rebound effect (During retraction, the contact line of PEO drops is known to retract an order of magnitude more slowly than for water). This suggests that the origin of the anti-rebound effect is a drop edge effect

$\ll 1,000$ s^{-1}). The fluid elements are also in compression rather than extension, making the stretching of molecules in the drop interior unlikely. A comparison of the fluid velocity in the bulk of the droplet with those values extracted from macroscopic observations of the contact line shows a dramatic difference between water and PEO drops. The motion of the contact line for droplets of pure water is similar to that of the bulk fluid. By contrast, the motion of the contact line for PEO drops is ~ 1 order of magnitude slower than that of the corresponding bulk velocity measurements (Smith and Bertola 2010). This difference implies that the difference between the two fluids lies solely at the droplet edge. A linear fit to the

retraction velocity data reveals initial velocity gradients for water and PEO drops of 107 ± 15 and 32 ± 17, respectively. If the drop edge were responsible for the anti-rebound effect, we would expect this to slow the fluid nearest the drop edge first. This is indeed what is observed in Figures 9 and 10. Data points near the centre of the drop are indistinguishable within error, whilst those near the edge show a small but measurable difference. The critical role of the contact line is supported by recent measurements of the dynamic contact angle of retracting drops (Smith and Bertola 2010; Bertola 2010) and direct visualisation of DNA, stretching at the receding drop edge (Smith and Bertola 2010). The anti-rebound phenomenon therefore cannot be a result of changes in the extensional viscosity of the drop.

4 Conclusions

A novel high speed microscopy technique to enable the visualisation and quantification of flows inside an impacting drop was successfully built and demonstrated. The technique was then applied to two different problems. Firstly, our measurements of the velocity field inside the lamella were used to confirm the Roisman-Yarin model for an impacting Newtonian droplet, spreading on a surface. Secondly, by comparing the fluid velocities inside impacting drops of water and 200 ppm PEO, we were able to exclude the extensional viscosity as a significant factor in the anti-rebound effect during both spreading and retraction stages.

References

Adrian RJ (1991) Particle-imaging techniques for experimental fluid mechanics. Annu Rev Fluid Mech 23:261–304

Adrian RJ (2005) Twenty years of particle image velocimetry. Exp Fluids 39(2):159–169

Bakshi S, Roisman IV, Tropea C (2007) Investigations on the impact of a drop onto a small spherical target. Phys Fluids 19:032102

Berberovic E, van Hinsberg NP, Jakirlic S, Roisman IV, Tropea C (2009) Drop impact onto a liquid layer of finite thickness: dynamics of cavity evolution. Phys Rev E 79(3):036306

Bergeron V, Bonn D, Martin JY, Vovelle L (2000) Controlling droplet deposition with polymer additives. Nature 405(6788):772

Bertola V (2003) Two-phase flows measurement techniques, in modelling and experimentation in two-phase flow. CISM Course Lect 450:281–323

Bertola V (2004) Drop impact on a hot surface: effect of a polymer additive. Exp Fluids 37(5):653–664

Bertola V (2009) An experimental study of bouncing Leidenfrost drops: comparison between Newtonian and viscoelastic liquids. Int J Heat Mass Transf 52(7):1411

Bertola V (2010) Effect of polymer additives on the apparent dynamic contact angle of impacting drops. Colloids Surf A Physicochem Eng Asp 363(1-5):135–140

Boffetta G, Mazzino A, Musacchio S, Vozella L (2010) Polymer heat transport enhancement in thermal convection: the case of Rayleigh–Taylor turbulence. Phys Rev Lett 104(18):184501

Crooks R, Cooper-White J, Boger DV (2001) The role of dynamic surface tension and elasticity on the dynamics of drop impact. Chem Eng Sci 56(19):5575

de Gennes PG (1974) Coil-stretch transition of dilute flexible polymers under ultrahigh velocity gradients. J Chem Phys 60(12):5030

Eggers J, Fontelos MA, Josserand C, Zaleski S (2010) Drop dynamics after impact ona solid wall:theory and simulations. Phys Fluids 22(6):062101

Fukai J, Zhao Z, Poulikakos D, Megaridis CM (1993) Modelling of the deformation of a liquid droplet impinging upon a flat surface. Phys Fluids A 5:2588–2599

Kang KH, Lee SJ, Lee CM, Kang IS (2004) Quantitative visualisation of flow inside an evaporating droplet using the ray tracing method. Meas Sci Technol 15(4):1104–1112

Keller A, Odell JA (1985) The extensibility of macromolecules in solutions: a new focus for macromolecular science. Colloids Polym Sci 263(3):181–201

Rein M (1993) Phenomena of liquid drop impact on solid and liquid surfaces. Fluid Dyn Res 12(2):61

Roisman IV (2009) Inertia dominated drop collisions. II. An analytical solution of the Navier-Stokes equations for a spreading viscous film. Phys Fluids 21:052104

Roisman IV, Rioboo R, Tropea C (2001) Normal impact of a liquid drop on a dry surface: model for spreading and receding. Proc R Soc Lond A 458:1411–1430

Rozkhov A, Prunet-Foch B, Vignes-Adler M (2003) Impact of drops of polymer solutions on small targets. Phys Fluids 15(7):2006

Sikalo S, Wilhelm HD, Roisman IV, Jakirlić S, Tropea C (2005) Dynamic contact angle of spreading droplets:experiments and simulations. Phys Fluids 17:062103

Smith MI, Bertola V (2010) Effect of polymer additives on the wetting of impacting droplets. Phys Rev Lett 104(15):154502

Tropea C, Yarin AL, Foss JF (2007) Springer handbook of fluid mechanics. Springer, New York

Westerweel J (1997) Fundamentals of digital particle image velocimetry. Meas Sci Technol 8(12):1379

Williams PA, English RJ, Blanchard RL, Rose SA, Lyons L, Whitehead M (2008) The influence of the extensional viscosity of very low concentrations of high molecular mass water-soluble polymers on atomisation and droplet impact. Pest Manag Sci 64(5):497

Yarin AL (2006) Drop impact dynamics: splashing, spreading, receding bouncing. Annu Rev Fluid Mech 38:159–194

Yarin AL, Weiss DA (1995) Impact of drops on solid surfaces: self-similar capillary waves, and splashing as a new type of kinematic discontinuity. J Fluid Mech 283:141–173

Yarin AL, Brenn G, Kastner O, Rensink D, Tropea C (1999) Evaporation of acoustically levitated droplets. J Fluid Mech 399:151–204